Atomistic understanding of zeolite nanosheets for water desalination

Jamali, Sayed; Vlugt, Thijs; Lin, Li-Chiang

DOI
10.1021/acs.jpcc.7b00214

Publication date
2017

Document Version
Final published version

Published in
The Journal of Physical Chemistry C

THE JOURNAL OF PHYSICAL CHEMISTRY C

Article

pubs.acs.org/JPCC

Atomistic Understanding of Zeolite Nanosheets for Water Desalination

Seyed Hossein Jamali,[†] Thijs J. H. Vlugt,[†] and Li-Chiang Lin*[,‡]

[†]Engineering Thermodynamics, Process & Energy Department, Faculty of Mechanical, Maritime, and Materials Engineering, Delft University of Technology, Leeghwaterstraat 39, 2628CB Delft, The Netherlands

[‡]William G. Lowrie Department of Chemical and Biomolecular Engineering, The Ohio State University, Columbus, Ohio 43210, United States

Supporting Information

ABSTRACT: Reverse osmosis constitutes a large portion of currently operating commercial water desalination systems. Employing membranes with large water fluxes while maintaining high salt rejection is of central importance in decreasing the associated energy consumption and costs. The ultrathin-film nature of zeolite nanosheets and their versatile pore structures provides great opportunities in desalination. To push forward the development of zeolite nanosheets for water desalination, nonequilibrium molecular dynamics simulations were carried out to systematically study zeolites as RO membranes and establish fundamental structure-performance relationships. We have identified that zeolite nanosheets can achieve a high salt rejection rate close to 100% while allowing nearly 2 orders of magnitude higher water permeability than currently available membranes. Moreover, the effects of the pore density, inclusion of cages, and free energy barrier on water permeability and salt rejection are unraveled, leading to important insights toward the rational design of novel zeolite membranes.

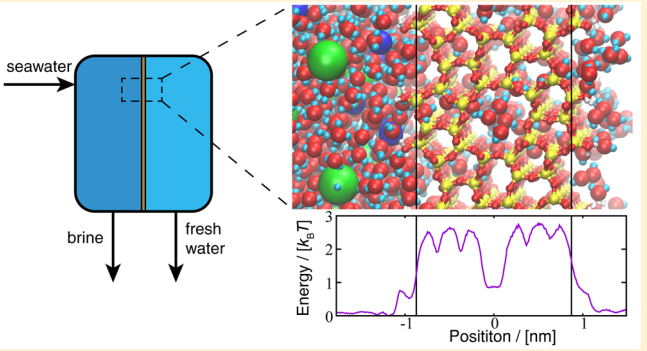

INTRODUCTION

In the past decades, the need for water desalination has increased significantly[1] and this need will become more pronounced due to the continuing population growth and economic development.[2] Among various methods to produce fresh water from saline sources, reverse osmosis (RO) is currently the most prevalent approach with a global market share of approximately 60%,[1] and polyamide-based RO membranes have been widely used.[3−5] The associated energy consumption and the cost of the process largely depend on the permeability of the RO membrane.[5] Cohen-Tanugi et al.[6] have recently shown that there will be 44% reduction in the number of pressure vessels or 15% reduction in the energy consumption of the seawater reverse osmosis (SWRO) desalination, provided that the permeability of membranes is improved 3-fold compared to the current polyamide-based membranes. The need for more fresh water requires new membranes to increase the flux of RO membranes while maintaining excellent salt rejection to make this process more energy and cost efficient. In the past few years, many types of novel materials have been investigated experimentally and/or computationally, and they have shown great promise as membranes in RO water desalination such as nanoporous graphene,[7−12] graphene oxide,[11−14] covalent triazine frameworks (CTFs),[15] MoS_2,[16] and graphyne.[17−19] A common feature of these candidates is the ultrathin-film nature of the material, highlighting the need for discovering ultrathin-film membranes. Furthermore, pore structures in these membranes can effectively block salt ions passage, leading to outstanding salt rejections.

Recently, considerable attention has been paid to layered zeolites with a thickness varying from one to several unit cells.[20−24] These systems possess short diffusion lengths, potentially overcoming diffusion and mass transfer limits. Various types of zeolites have been synthesized in the nanosheet form with different possible interlayer linkers[22,25−30] with an aim at targeting various catalytic systems such as isomerization and hydrocracking,[31−35] selective formation of molecules,[29,36−39] and epoxidation reactions.[40−42] Although zeolite nanosheets have been also considered for adsorption[43−45] and membrane[46] separation systems, zeolite nanosheets specifically as RO membranes for water desalination have been greatly overlooked in the literature. The small thickness of layered zeolites (i.e., short diffusion distance) along with their excellent chemical and physical resistance make zeolite nanosheets a promising type of RO membrane materials in water desalination. It is also anticipated that the hydrophilic nature (i.e., silanol (SiOH) groups on the surface) of zeolite nanosheets can render these membranes better resistant to

Received: January 8, 2017
Revised: March 12, 2017
Published: March 17, 2017

DOI: 10.1021/acs.jpcc.7b00214
J. Phys. Chem. C XXXX, XXX, XXX−XXX

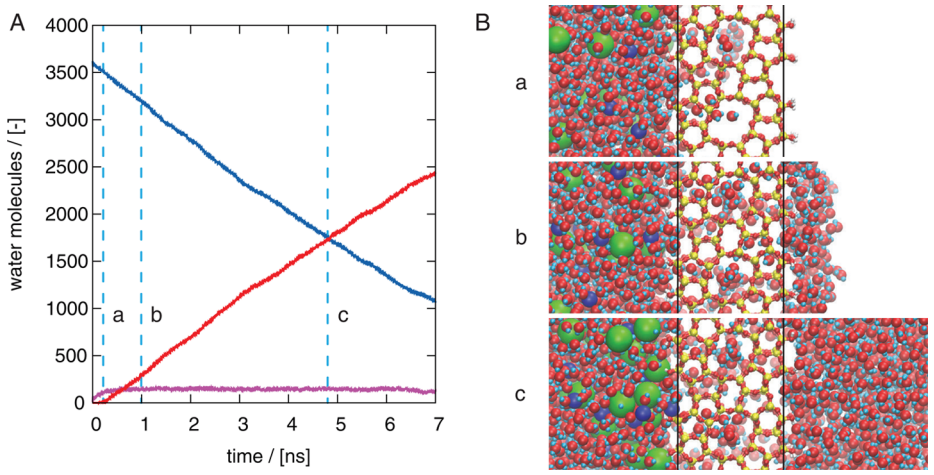

Figure 1. (A) The number of water molecules in the feed (blue), inside the membrane (magenta), and on the permeate side (red) as a function of time for a typical simulation. (B) Snapshots of the simulation at time steps a, b, and c. The vertical black lines show the surfaces of zeolites using the position of the furthest silicon atom from the center of the zeolite.

biofouling.[47] Moreover, 232 distinct zeolite topologies have been identified and included in the International Zeolite Associations (IZA) database to date,[48] while millions more have been theoretically predicted.[49−51] Such a large materials space further provides tremendous opportunities for zeolite membranes in water desalination.

Despite the potential of zeolite nanosheets in water desalination applications, no experimental investigation of zeolite nanosheets as RO membranes has been reported to the best of our knowledge. Experimental studies on desalination using zeolites focused primarily on bulk zeolites[52−63] or thin-film nanocomposites (TFN) in which zeolite nanoparticles are incorporated in thin film polyamide/polymer membranes.[64−69] These systems are inherently different from the zeolite nanosheets, and these experimental studies are also limited to very few zeolites. A similar situation applies to computational studies reported to date in the literature. The computational investigation of zeolite nanosheets for their desalination performance remains limited. While some studies attempted to address the diffusion of water molecules or salt ions in bulk zeolites,[70,71] few were carried out to study zeolites in a form of nanosheet membrane.[72−74] Despite the vast material space of zeolites, only three zeolites (i.e., MFI, FAU, and LTA) have been investigated.

To push forward the development of zeolite nanosheets for water desalination, it remains of utmost importance to establish a fundamental structure−performance relationship, as an important basis for the optimal design of zeolite RO membranes. To achieve this, systematically studying a number of materials with a wide range of structural characteristics is needed. In this study, state-of-the-art molecular dynamics (MD) techniques are used as an efficient approach to address this missing knowledge.

SIMULATION DETAILS

Nonequilibrium MD simulations are used to investigate the water permeability and salt rejection of zeolite nanosheet membranes. Simulations are carried out in LAMMPS, a molecular dynamics simulation package.[75] A solution of water and salt is pressurized by a piston to push water molecules through a membrane. The position of water molecules and salt ions is recorded during the simulation, which is postprocessed to calculate the water permeability and salt rejection of the studied zeolite nanosheet. A sample chart of water permeation through an MFI nanosheet membrane along with three typical snapshots of the system is illustrated in Figure 1. This figure shows the evolution of the number of water molecules in the feed, membrane, and permeate during the simulation. As water permeates through the membrane, the number of water molecules in the membrane reaches a constant and water molecules accumulate on the permeate side. Water flux through the membrane is calculated from the slope of water accumulation on the permeate side (the red line in Figure 1A). The water flux is computed when at least a layer of water molecules is present on the surface of the permeate and the number of permeated water molecules is less than that of the feed. This corresponds to a time span between points b and c in Figure 1A. The permeability of a membrane is defined as the water flux divided by the pressure difference (i.e., the exerted pressure minus the osmotic pressure) and the cross-sectional area. The salt rejection is defined as the ratio of the number of passed ion pairs to the initial number on the feed side when half of the water molecules permeate to the permeate side (corresponding to point c in Figure 1A).

The initial configuration of water molecules and salt ions in our simulations is constructed in several steps. A zeolite slab with a total thickness of approximately 25 Å (within a range of 20−30 Å) in the permeation direction is used as the active reverse osmosis membrane layer. The surface of this zeolite slab is functionalized with hydroxyl (OH) groups, that is, all dangling bonds of silicon atoms are saturated with hydroxyl groups. The silanol (SiOH) group is one of the most abundant surface functionalizing groups of zeolites. The hydrogen bond of the siloanol groups provides the required interconnection force to stack zeolite nanosheets to construct a controlled multilayer zeolite nanosheet.[22,23] An electrically neutral mixture of sodium and chloride ions along with water molecules is added to one side of the membrane by using the Autoionize plugin in VMD.[76] This saline solution with a concentration of 1.0 M, almost twice the salt concentration of seawater, is employed to achieve better statistics of the ability of membranes to reject salt ions within the short MD time scale (i.e., on the order of 10 ns). A similar concentration has been also adopted by other computational studies.[7,15,72] A piston is

DOI: 10.1021/acs.jpcc.7b00214
J. Phys. Chem. C XXXX, XXX, XXX−XXX

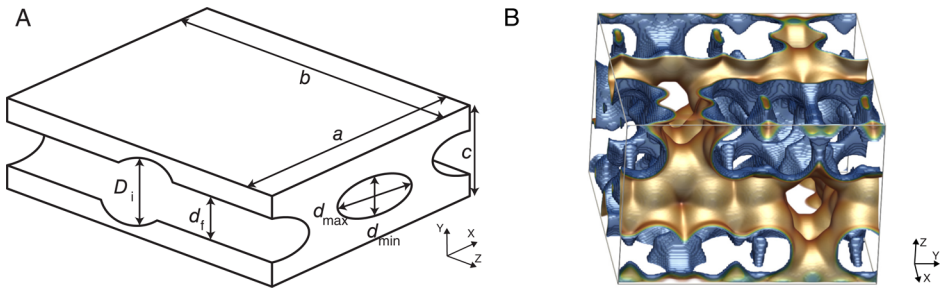

Figure 2. (A) Schematic representation of a one-dimensional zeolite unit cell with a pore density of 2 channels per unit cell in the *xy* plane. d_f and D_i are the PLD and the largest included sphere diameters, respectively. d_{min} and d_{max} are, respectively, the minimum and maximum diameter of that channel. (B) MFI, a zeolite with multidimensional channels, has a interconnected network of straight and zigzag channels in the *y*- and *x*-directions that are shown in yellow. Similar structural characteristics can be defined.

placed on the feed side, and a constant force is applied on the piston to modulate the transmembrane pressure. The applied force exerts an average constant pressure of 300 MPa on the solution. The high pressure applied on the piston reduces the sensitivity of the driving force to the feed concentration and the water flux subsequently remains almost constant while the feed is depleted. Furthermore, applying such a high pressure can achieve more accurate statistics within the short MD time scale.

The force fields used in our simulations are chosen to be fully compatible between the membrane, water molecules, and salt ions. The potential parameters for both the inside and the surface of the zeolite nanosheet are adopted from the work of Emami et al.[77] This force field has been applied to study zeolites with a wide range of hydroxyl group densities (the SiOH density on the surface of a zeolite) and pHs. Because this force field only considers bond stretching and bond angle bending of the silanol groups on the surface, it is less computationally intensive compared to other proposed force fields such as the work of Cruz-Chu et al.[78] or Lopes et al.[79] Water molecules are modeled using the TIP3P model. The force field for ions is taken from the work of Joung and Cheatham[80] with parameters compatible to the TIP3P model. The force field parameters for bond stretching, bond angle bending, and all nonbonded potentials are summarized in the Supporting Information.

All short-range nonbonded interactions are truncated and shifted to zero at a cutoff radius of 12.0 Å. For long-range Coulombic interactions, the particle−particle particle−mesh (pppm) method with a relative accuracy of 10^{-6} is used. For dissimilar atoms, the Lorentz−Berthelot mixing rules are applied.[81] The 1−4 intramolecular nonbonded interactions are included and scaled by 0.5 and 0.8333 for Lennard-Jones and Coulombic interactions, respectively.[77] The bulk part of the studied zeolite nanosheet (i.e., nonsurface part) is assumed to be rigid for simplicity. As a result, the silicon and oxygen atoms do not move during the simulation although the structure of bulk zeolites might slightly vary while loaded with water molecules.[82] The effect of structural flexibility on the separation performance of zeolites has been found to be negligible,[72] and it is therefore anticipated that the outcomes of our study will not be significantly affected by assuming a rigid structure. In this study, the atomistic structure of the bulk part of zeolites are taken from the IZA database.[48] The equations of motion for water molecules, sodium and chloride ions, and atoms of the hydroxyl groups on the surface of the membrane are integrated using the Verlet algorithm.[81] The Nosé−Hoover thermostat is used to regulate the temperature at 298 K in an NVT ensemble. It is known that this thermostat does not significantly influence the diffusion of water.[71] The rigid bonds and bond angles of water are considered by the means of the SHAKE algorithm. Four independent simulations with uncorrelated initial configurations have been carried out for each studied zeolite.

RESULTS AND DISCUSSION

A set of nonequilibrium MD simulations for a total number of 27 zeolite structures were carried out to investigate saline water permeation through zeolite nanosheets. Out of this number of zeolites, 15 zeolites have one-dimensional channels, 8 zeolites have multidimensional channels, and 4 have cage-containing channels that connects cages to each other. All these zeolites studied herein are adopted from the IZA database,[48] and we have only chosen to study materials that have an orthorhombic unit cell for simplification. Such unit cells allow us to use a rectangular simulation box with periodic boundaries. The pore-limited diameter (PLD or d_f) of these zeolites, which represents the diameter of the largest sphere that can transverse the channel, varies between 4.0 and 7.5 Å. We note that a water molecule has a kinetic diameter of approximately 2.8 Å; water molecules are therefore less likely to permeate through channels with PLDs smaller than or close to this value.[83] Generally speaking, the transport properties of a zeolite membrane can be a function of various geometrical parameters, some of which are presented in Figure 2A for a unit cell of a schematic zeolite. The PLD, however, is predicted to be of utmost importance for the diffusion properties such as the water permeation rate.[84]

Water Permeability. We plot the water flux per cross-sectional area versus the PLD as shown in Figure 3. A connection between water flux and the PLD is found but it is rather scattered. As the density of channels per unit area varies from one zeolite to another, it is more sensible to take the number of channels per unit area into account. As expected, the water permeability per channel shows a more pronounced correlation with the PLD. Overall, we can observe that the water permeability generally increases with an increase in the PLD. As shown in Figure 3, the water permeability of one layer of zeolite nanosheet can be as high as 40 L/day/cm^2/MPa. For comparison, a layer of nanoporous graphene functionalized with hydrogen or hydroxyl groups have water permeabilities up to 60 and 140 L/day/cm^2/MPa, respectively.[7] Two-dimensional covalent triazine frameworks (CTFs) show also high water permeability up to 65 L/day/cm^2/MPa depending on the pore structure.[15] Zeolite nanosheets have similar water permeabilities compared to other novel ultrathin-film membranes, which again demonstrates the importance of this type of membranes. In practice, several layers of these two-dimensional

DOI: 10.1021/acs.jpcc.7b00214
J. Phys. Chem. C XXXX, XXX, XXX−XXX

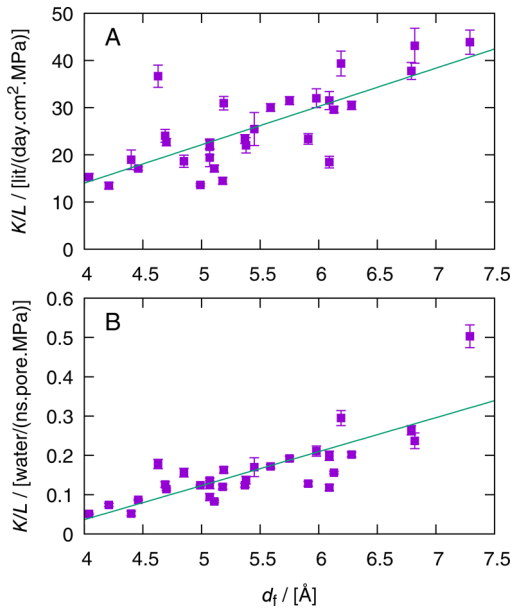

Figure 3. Water permeability (K/L) of studied zeolites per area (A) and per channel (B) as a function of the PLD. The permeability per pore has units of number of water molecules permeated per nanoseconds, per pore, per pressure difference. The lines serve as guides to the eye. These data are available in the Supporting Information.

sheets are superimposed, resulting in multilayered structures, or one layer of several unit cells are used.[23] A multilayered structure can potentially lead to improved structural strength and better ability to reject salt but, at the same time, reduce the water flux.[10] If the water permeability decreases reciprocally with the thickness of the effective membrane,[72] a currently available zeolite nanosheet of 100 nm thickness may have a permeability as high as 1.3 L/day/cm^2/MPa, which is still a significant improvement compared to the conventional systems with water permeabilities, ranging from 0.03 to 0.2 L/day/cm^2/MPa.[5] This means that a substantial reduction in the number of pressure vessels and energy consumption can be achieved.[6] Nonetheless, to advance membranes using zeolite nanosheets, developing thinner stacked membranes should be an important subject of future studies.

Although a relationship between the water permeability and the PLD has been established (Figure 3), this simple descriptor is still unable to fully explain water permeation in the membranes (i.e., notable variation in permeabilities at a fixed PLD). To better understand this variation, the free energy landscape of water in zeolites was computed, which is a critically determining factor to describe the transport of water molecules. In this study, we use the average density of water at each cross section of the membrane, computed from the configurations stored during the simulations, to obtain the free energy landscape of water inside a zeolite nanosheet. The free energy landscape of several zeolites with one-dimensional channels that have permeabilities different than the average permeability of a PLD is shown in Figure 4. The zeolites that have higher water permeabilities than the average are AEL, PSI, and SAF with pore-limited diameters of 4.63, 4.85, and 6.19 Å, respectively. The zeolites with lower water permeabilities are JRY, TON, and EZT with PLDs of 4.40, 5.11, and 6.13 Å. For the zeolites with the PLDs between 4.40 and 5.11 Å, AEL has the highest water permeability followed by PSI, TON, and JRY. Moreover, SAF has a water permeability per channel twice that of EZT although both of them have similar PLDs. Overall as shown in Figure 4, these membranes possess a large free energy barrier for water permeation on their surfaces where are filled with silanol (SiOH) groups. Interestingly, we found that such a barrier is not evidently correlated to the difference in water permeabilities. As the surface of the membrane is filled with

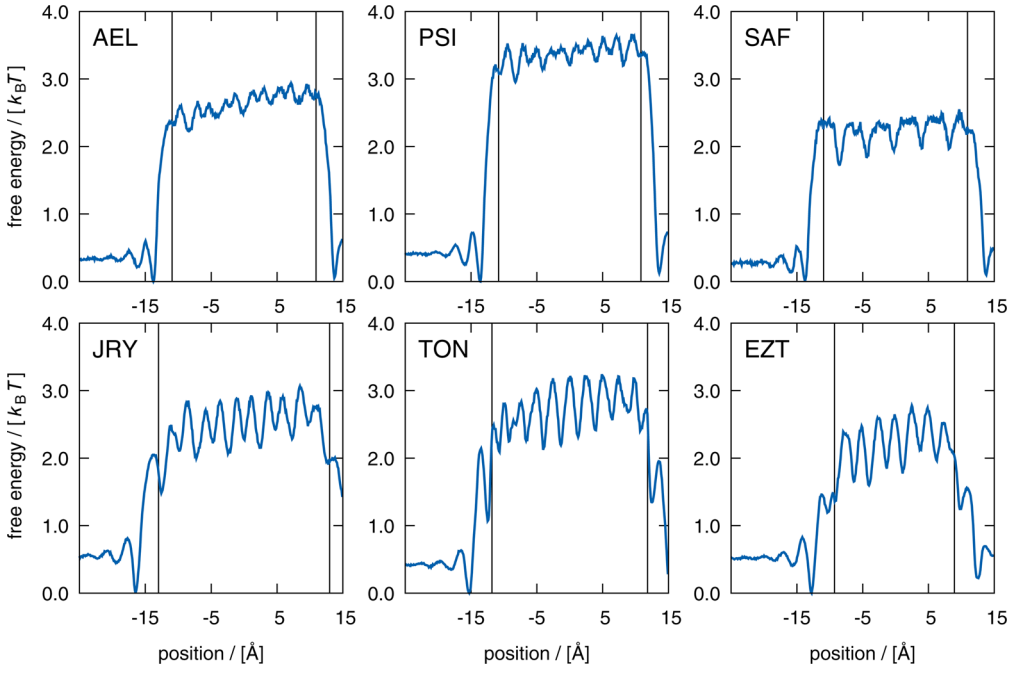

Figure 4. Free energy profiles of zeolites with one-dimensional channels. The profiles in the upper panel have larger permeabilities while those in the lower panel have smaller permeabilities than the average at a given PLD. The vertical lines show the surfaces of zeolites using the position of the furthest silicon atom from the center. The minimum free energy is shifted to zero.

DOI: 10.1021/acs.jpcc.7b00214
J. Phys. Chem. C XXXX, XXX, XXX−XXX

hydroxyl groups, this observation suggests that the density of hydroxyl groups may not have a pronounced influence on the water permeability. Instead, the transport barrier inside the membrane appears to control the diffusion of water molecules. Membranes with higher permeabilities are those structures with the lowest free energy barrier inside the channel (AEL and PSI versus JRY and TON) along with a smaller number of barriers or jumps (EZT versus SAF). For zeolites with multidimensional channels, a similar behavior was observed as well but the free energy landscape is more complex than zeolites with one-dimensional channels due to the interconnected channels in different directions (Figure 2B).

It is worth mentioning that FAU (with a PLD of 7.35 Å) has the smallest free energy barrier (1.5 k_BT) on its surface and inside, which makes its large permeability per channel possible (see Figure 3B). However, because the pore density per area of FAU is half of the density of ATS, whose PLD is comparable to FAU's PLD but possesses a higher transport free energy barrier, the permeability per area of these two zeolites are the same. Likewise, it was shown that AEL and PSI have a high water permeability per channel due to their favorable free energy landscape, but AEL has a two times more water permeability per area than PSI because of its larger pore density (0.80 versus 0.46 pore/nm^2). Hence, our results clearly suggest that the density of channels plays an important role in quantitatively determining water flux in zeolites.

Salt Rejection. To enable effective desalination, membranes have to be nearly semipermeable (i.e., blocking salt ions from passage). Sodium and chloride ions have first hydrated shell radii of 2.356 and 3.187 Å, respectively.[85] These radii can be reproduced by the force field of salt ions and the TIP3P water molecule model,[80] and they have been calculated to be 2.38 and 3.13 Å. Zeolites with PLDs larger than 6.4 Å (twice 3.187 Å) may not be appealing candidates for water desalination due to the possible permeation of both sodium and chloride. To quantify the salt rejection of a membrane, we use the number of passed ion pairs from the beginning of a simulation until the number of water molecules on both sides of the membrane is equal. This corresponds to the time when the lines for the number of water molecules in the feed and the permeate sides cross each other (Figure 1). In Figure 5, the salt rejection is shown as a function of the PLD of the zeolites. Zeolites with PLDs below 5.5 Å (between the first hydrated shell diameters of sodium and chloride) show a salt rejection very close to 100%. At this point, it should be pointed out that higher applied pressures normally lead to a relatively lower salt rejection. As pointed out previously, a high pressure of 300 MPa is applied herein to obtain better statistics within the time scale of an MD simulation. As a result, under practical conditions, salt rejection might be higher.[7] As a comparison, Cohen-Tanugi and Grossman[7] showed that a layer of nanoporous graphene can effectively hinder salt ions when the nanoporous graphene has a pore size of 5.5 Å (i.e., PLD = 5.5 Å). This value is similar to the value of maximum PLD we obtained here. Similarly, comparing the result to other classes of materials, it was found that CTFs with an effective radius of approximately 3 Å exhibit salt rejections of 96% and 100% depending on the chemistry of the pores.[15] Accordingly, it was suggested that a PLD ranging from 5.5 to 6.0 Å seemingly generally defines the limits on how large the PLD needed to be in order to effectively reject salt ions. We note that, however, other factors (e.g., topologies, pore chemistries, and so forth) could also affect the salt rejection.

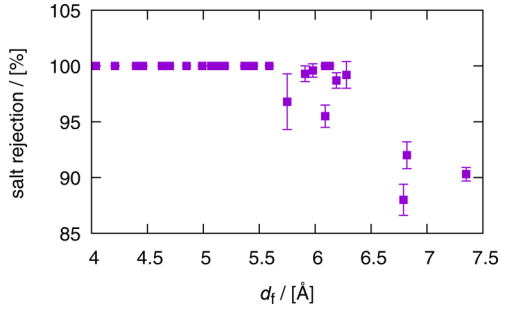

Figure 5. Salt rejection as a function of the PLD in the studied zeolites. These data are available in the Supporting Information.

In addition to the aforementioned PLD criterion, we found that the cross-sectional area of a zeolite channel, calculated from the area of an ellipse with major and minor radii equal to d_{max} and d_{min} (Figure 2), can be another factor to identify zeolites with high salt rejections. The area of the first hydrated shell of sodium and chloride ions are approximately 18 and 31 Å^2, respectively. It is anticipated that channels with cross-sectional areas less than 18 Å^2 can potentially block ions, resulting in a nearly 100% rejection rate. In contrast, zeolites with channel cross-sectional areas in the vicinity of 31 Å^2 or above may have a low salt rejection. From our simulations, it was found that all zeolites with a salt rejection less than 99% have a channel cross-sectional area larger than or equal to 30 Å^2. However, not all zeolites whose channel cross-sectional area is larger than 30 Å^2 show low salt rejection, so other factors and the energy barrier inside the channel against the ion transport play a role.

It is interesting to compare two specific zeolites: SSY and SAF. As listed in the Supporting Information, they have PLDs of 5.75 and 6.19 Å, respectively. Their one-dimensional channels have minimum widths of 5.0 and 5.6 Å, as well as maximum widths of 7.6 and 8.5 Å, corresponding to channel cross-sectional areas of 30 and 37 Å^2, respectively. SAF has a 25% higher water permeability than SSY due to its larger channel area and PLD. However, SAF was found to have a higher salt rejection (99%) than SSY (97%). This may seem less intuitive but this observation may be attributed to the effect of cages. The largest included sphere diameters (D_i) of SSY and SAF (i.e., the maximum diameter of a sphere that can be fitted in the pores of a zeolite; see Figure 2A) are 7.10 and 6.66 Å, respectively. Although both membranes have PLDs larger than the first hydrated shell diameter of sodium and smaller than that of chloride, SAF has a similar included diameter compared to the hydrated shell of chloride. When a chloride ion and its hydrated shell permeate through SAF, the hydrated ion could fit tightly to the cage with strong interactions between the hydrated ion and the cage surface and therefore increase the overall transport barrier. Hence, chloride ions are anticipated to experience more resistance to permeation in SAF than SSY. This insight can be important to the design of novel zeolite nanosheet membranes, suggesting that the inclusion of cages with a right size may be exploited to manipulate membranes' salt rejection without sacrificing their water permeability.

Several zeolites that have been already synthesized in two-dimensional nanosheet forms are summarized in the review by Roth et al.[22] According to the established structure−performance relationship, four of these two-dimensional zeolites appeal to be promising for water desalination: OKO, MWW, MFI, and

DOI: 10.1021/acs.jpcc.7b00214
J. Phys. Chem. C XXXX, XXX, XXX−XXX

FER. It is predicted that OKO has the highest water permeation among these zeolites due to the large PLDs of the two channels of OKO (5.1 and 5.9 Å) and their corresponding high pore densities (0.60 and 0.67 pore/nm^2). However, the salt rejection of OKO in the direction with a PLD of 5.9 Å might be slightly less ideal due to the rather large PLD together with a cross-sectional area of 31 Å^2 and an included diameter of 6.7 Å. These values are at the limit we identified earlier for efficient salt rejection. Future investigations are needed to determine precisely the transport properties of this particular channel. Notwithstanding, the other direction possessing a PLD of 5.1 Å can provide a high water permeability while the smaller channel cross-sectional area (22.5 Å^2) can prevent the permeation of salt ions.

We note that the results obtained in this study are for hydrophobic zeolites without defects inside the membrane. Hydrophobic zeolites typically show a large infiltration pressure in the bulk structure.[86] The existence of defects or nonframework cations increases the hydrophilicity of a zeolite, which can increase the solubility of water while also potentially deteriorating diffusion properties.[87] Investigating zeolites with defects or nonframework cations is an important subject of future studies.

CONCLUSION

In this study, we used nonequilibrium MD simulations to calculate the water permeability and salt rejection of 27 zeolites. The results clearly show that zeolite nanosheets possess promising separation performance, making them potential membrane candidates in water desalination. Furthermore, the results obtained herein have provided a set of guidelines for the design of novel RO zeolite nanosheet membranes. In this work, specifically, we have identified three important selection criteria and design principles for choosing appropriate zeolite nanosheets for water desalination. First, a recommended zeolite may have a large but smaller than 5.5 Å PLD. We note that, however, channels with larger PLDs may still be promising for effective separations but other effects of the channel structure on salt rejection should be taken into account (e.g., the cross-sectional area and the shape of channels). Second, zeolites possessing a larger channel density are beneficial for the water permeation. Third, the salt rejection may be enhanced when the included cages have a comparable size to the first hydrated shell diameter of chloride (i.e., 6.5 Å). With this finding at our disposal, one could potentially manipulate structures by designing channels with cages at a proper size to improve salt rejections without compromising water permeability.

ASSOCIATED CONTENT

Supporting Information

The Supporting Information is available free of charge on the ACS Publications website at DOI: 10.1021/acs.jpcc.7b00214.

Details of the adopted force field, as well as tables and figures containing the summarized results of this work and the free energy landscapes of water in all studied zeolites (PDF)

AUTHOR INFORMATION

Corresponding Author

*E-mail: lin.2645@osu.edu.

ORCID

Thijs J. H. Vlugt: 0000-0003-3059-8712

Li-Chiang Lin: 0000-0002-2821-9501

Notes

The authors declare no competing financial interest.

ACKNOWLEDGMENTS

This work was sponsored by NWO Exacte Wetenschappen (Physical Sciences) for the use of supercomputer facilities, with financial support from the Nederlandse Organisatie voor Wetenschappelijk Onderzoek (Netherlands Organisation for Scientific Research, NWO). The authors also gratefully acknowledge the Ohio Supercomputer Center[88] for providing computational resources. T.J.H.V. acknowledges NWO−CW (Chemical Sciences) for a VICI grant.

REFERENCES

(1) Ghaffour, N.; Missimer, T. M.; Amy, G. L. Technical review and evaluation of the economics of water desalination: Current and future challenges for better water supply sustainability. *Desalination* **2013**, *309*, 197−207.

(2) Vörösmarty, C. J.; Green, P.; Salisbury, J.; Lammers, R. B. Global water resources: Vulnerability from climate change and population growth. *Science* **2000**, *289*, 284−288.

(3) Mohammad, A.; Teow, Y.; Ang, W.; Chung, Y.; Oatley-Radcliffe, D.; Hilal, N. Nanofiltration membranes review: Recent advances and future prospects. *Desalination* **2015**, *356*, 226−254.

(4) Greenlee, L. F.; Lawler, D. F.; Freeman, B. D.; Marrot, B.; Moulin, P. Reverse osmosis desalination: Water sources, technology, and today's challenges. *Water Res.* **2009**, *43*, 2317−2348.

(5) Pendergast, M. M.; Hoek, E. M. A review of water treatment membrane nanotechnologies. *Energy Environ. Sci.* **2011**, *4*, 1946−1971.

(6) Cohen-Tanugi, D.; McGovern, R. K.; Dave, S. H.; Lienhard, J. H.; Grossman, J. C. Quantifying the potential of ultra-permeable membranes for water desalination. *Energy Environ. Sci.* **2014**, *7*, 1134−1141.

(7) Cohen-Tanugi, D.; Grossman, J. C. Water desalination across nanoporous graphene. *Nano Lett.* **2012**, *12*, 3602−3608.

(8) Surwade, S. P.; Smirnov, S. N.; Vlassiouk, I. V.; Unocic, R. R.; Veith, G. M.; Dai, S.; Mahurin, S. M. Water desalination using nanoporous single-layer graphene. *Nat. Nanotechnol.* **2015**, *10*, 459−464.

(9) Cohen-Tanugi, D.; Grossman, J. C. Nanoporous graphene as a reverse osmosis membrane: Recent insights from theory and simulation. *Desalination* **2015**, *366*, 59−70.

(10) Cohen-Tanugi, D.; Lin, L.-C.; Grossman, J. C. Multilayer nanoporous graphene membranes for water desalination. *Nano Lett.* **2016**, *16*, 1027−1033.

(11) Dervin, S.; Dionysiou, D. D.; Pillai, S. C. 2D nanostructures for water purification: Graphene and beyond. *Nanoscale* **2016**, *8*, 15115−15131.

(12) You, Y.; Sahajwalla, V.; Yoshimura, M.; Joshi, R. K. Graphene and graphene oxide for desalination. *Nanoscale* **2016**, *8*, 117−119.

(13) Mi, B. Graphene oxide membranes for ionic and molecular sieving. *Science* **2014**, *343*, 740−742.

(14) Lin, L.-C.; Grossman, J. C. Atomistic understandings of reduced graphene oxide as an ultrathin-film nanoporous membrane for separations. *Nat. Commun.* **2015**, *6*, 8335.

(15) Lin, L.-C.; Choi, J.; Grossman, J. C. Two-dimensional covalent triazine framework as an ultrathin-film nanoporous membrane for desalination. *Chem. Commun.* **2015**, *51*, 14921−14924.

(16) Heiranian, M.; Farimani, A. B.; Aluru, N. R. Water desalination with a single-layer MoS_2 nanopore. *Nat. Commun.* **2015**, *6*, 8616.

(17) Xue, M.; Qiu, H.; Guo, W. Exceptionally fast water desalination at complete salt rejection by pristine graphyne monolayers. *Nanotechnology* **2013**, *24*, 505720.

(18) Zhu, C.; Li, H.; Zeng, X. C.; Wang, E. G.; Meng, S. Quantized water transport: ideal desalination through graphyne-4 membrane. *Sci. Rep.* **2013**, *3*, 3163.

DOI: 10.1021/acs.jpcc.7b00214
J. Phys. Chem. C XXXX, XXX, XXX−XXX

(19) Kou, J.; Zhou, X.; Lu, H.; Wu, F.; Fan, J. Graphyne as the membrane for water desalination. *Nanoscale* **2014**, *6*, 1865−1870.
(20) Varoon, K.; Zhang, X.; Elyassi, B.; Brewer, D. D.; Gettel, M.; Kumar, S.; Lee, J. A.; Maheshwari, S.; Mittal, A.; Sung, C.-Y.; et al. Dispersible exfoliated zeolite nanosheets and their application as a selective membrane. *Science* **2011**, *334*, 72−75.
(21) Zhang, X.; Liu, D.; Xu, D.; Asahina, S.; Cychosz, K. a.; Agrawal, K. V.; Al Wahedi, Y.; Bhan, A.; Al Hashimi, S.; Terasaki, O.; et al. Synthesis of self-pillared zeolite nanosheets by repetitive branching. *Science* **2012**, *336*, 1684−1687.
(22) Roth, W. J.; Nachtigall, P.; Morris, R. E.; Čejka, J. Two-dimensional zeolites: current status and perspectives. *Chem. Rev.* **2014**, *114*, 4807−4837.
(23) Tsapatsis, M. 2-dimensional zeolites. *AIChE J.* **2014**, *60*, 2374−2381.
(24) Xu, L.; Sun, J. Recent advances in the synthesis and application of two-dimensional zeolites. *Adv. Energy Mater.* **2016**, *6*, 1600441.
(25) Choi, M.; Na, K.; Kim, J.; Sakamoto, Y.; Terasaki, O.; Ryoo, R. Stable single-unit-cell nanosheets of zeolite MFI as active and long-lived catalysts. *Nature* **2009**, *461*, 828−828.
(26) Dhainaut, J.; Daou, T. J.; Bidal, Y.; Bats, N.; Harbuzaru, B.; Lapisardi, G.; Chaumeil, H.; Defoin, A.; Rouleau, L.; Patarin, J. One-pot structural conversion of magadiite into MFI zeolite nanosheets using mononitrogen surfactants as structure and shape-directing agents. *CrystEngComm* **2013**, *15*, 3009.
(27) Díaz, U.; Corma, A. Layered zeolitic materials: An approach to designing versatile functional solids. *Dalt. Trans.* **2014**, *43*, 10292.
(28) Chen, H. L.; Li, S. W.; Wang, Y. M. Synthesis and catalytic properties of multilayered MEL-type titanosilicate nanosheets. *J. Mater. Chem. A* **2015**, *3*, 5889−5900.
(29) Sun, Q.; Wang, N.; Guo, G.; Yu, J. Ultrafast synthesis of nano-sized zeolite SAPO-34 with excellent MTO catalytic performance. *Chem. Commun.* **2015**, *51*, 16397−16400.
(30) Luo, Y.; Wang, Z.; Jin, S.; Zhang, B.; Sun, H.; Yuan, X.; Yang, W. Synthesis and crystal growth mechanism of ZSM-22 zeolite nanosheets. *CrystEngComm* **2016**, *18*, 5611−5615.
(31) Verheyen, E.; Jo, C.; Kurttepeli, M.; Vanbutsele, G.; Gobechiya, E.; Korányi, T. I.; Bals, S.; Van Tendeloo, G.; Ryoo, R.; Kirschhock, C. E.; et al. Molecular shape-selectivity of MFI zeolite nanosheets in n-decane isomerization and hydrocracking. *J. Catal.* **2013**, *300*, 70−80.
(32) Ren, Z.; Li, B.; Yue, L.; Wu, N.; Lv, K.; Han, C.; Liu, J. Hierarchical porous nano-MFI zeolite-pillared montmorillonite clay synthesized by recrystallization for hydrocracking of residual oil. *RSC Adv.* **2015**, *5*, 46104−46108.
(33) Ren, L.; Guo, Q.; Kumar, P.; Orazov, M.; Xu, D.; Alhassan, S. M.; Mkhoyan, K. A.; Davis, M. E.; Tsapatsis, M. Self-pillared, single-unit-cell Sn-MFI zeolite nanosheets and their use for glucose and lactose isomerization. *Angew. Chem., Int. Ed.* **2015**, *54*, 10848−10851.
(34) Xiao, X.; Zhang, Y.; Jiang, G.; Liu, J.; Han, S.; Zhao, Z.; Wang, R.; Li, C.; Xu, C.; Duan, A.; et al. Simultaneous realization of high catalytic activity and stability for catalytic cracking of n-heptane on highly exposed (010) crystal planes of nanosheet ZSM-5 zeolite. *Chem. Commun.* **2016**, *52*, 10068−10071.
(35) Ji, Y.; Shi, B.; Yang, H.; Yan, W. Synthesis of isomorphous MFI nanosheet zeolites for supercritical catalytic cracking of n-dodecane. *Appl. Catal., A* **2017**, *533*, 90−98.
(36) Hu, S.; Shan, J.; Zhang, Q.; Wang, Y.; Liu, Y.; Gong, Y.; Wu, Z.; Dou, T. Selective formation of propylene from methanol over high-silica nanosheets of MFI zeolite. *Appl. Catal., A* **2012**, *445*−*446*, 215−220.
(37) Kim, W.; Ryoo, R. Probing the catalytic function of external acid sites located on the MFI nanosheet for conversion of methanol to hydrocarbons. *Catal. Lett.* **2014**, *144*, 1164−1169.
(38) Kim, Y.; Kim, J.-C.; Jo, C.; Kim, T.-W.; Kim, C.-U.; Jeong, S.-Y.; Chae, H.-J. Structural and physicochemical effects of MFI zeolite nanosheets for the selective synthesis of propylene from methanol. *Microporous Mesoporous Mater.* **2016**, *222*, 1−8.
(39) Yutthalekha, T.; Wattanakit, C.; Warakulwit, C.; Wannapakdee, W.; Rodponthukwaji, K.; Witoon, T.; Limtrakul, J. Hierarchical FAU-type zeolite nanosheets as green and sustainable catalysts for benzylation of toluene. *J. Cleaner Prod.* **2017**, *142*, 1244−1251.
(40) Na, K.; Jo, C.; Kim, J.; Ahn, W.-S.; Ryoo, R. MFI titanosilicate nanosheets with single-unit-cell thickness as an oxidation catalyst using peroxides. *ACS Catal.* **2011**, *1*, 901−907.
(41) Wang, J.; Xu, L.; Zhang, K.; Peng, H.; Wu, H.; Jiang, J.-g.; Liu, Y.; Wu, P. Multilayer structured MFI-type titanosilicate: Synthesis and catalytic properties in selective epoxidation of bulky molecules. *J. Catal.* **2012**, *288*, 16−23.
(42) Li, C.-G.; Lu, Y.; Wu, H.; Wu, P.; He, M. A hierarchically core/shell-structured titanosilicate with multiple mesopore systems for highly efficient epoxidation of alkenes. *Chem. Commun.* **2015**, *51*, 14905−14908.
(43) Schick, J.; Daou, T. J.; Caullet, P.; Paillaud, J.-L.; Patarin, J.; Mangold-Callarec, C. Surfactant-modified MFI nanosheets: a high capacity anion-exchanger. *Chem. Commun.* **2011**, *47*, 902−904.
(44) Schnell, S. K.; Wu, L.; Koekkoek, A. J. J.; Kjelstrup, S.; Hensen, E. J. M.; Vlugt, T. J. H. Adsorption of Argon on MFI Nanosheets: Experiments and simulations. *J. Phys. Chem. C* **2013**, *117*, 24503−24510.
(45) Kabalan, I.; Rioland, G.; Nouali, H.; Lebeau, B.; Rigolet, S.; Fadlallah, M.-B.; Toufaily, J.; Hamiyeh, T.; Daou, T. J. Synthesis of purely silica MFI-type nanosheets for molecular decontamination. *RSC Adv.* **2014**, *4*, 37353.
(46) Hu, Y.; Wei, J.; Liang, Y.; Zhang, H.; Zhang, X.; Shen, W.; Wang, H. Zeolitic imidazolate framework/graphene oxide hybrid nanosheets as seeds for the growth of ultrathin molecular sieving membranes. *Angew. Chem., Int. Ed.* **2016**, *55*, 2048−2052.
(47) Kochkodan, V.; Hilal, N. A comprehensive review on surface modified polymer membranes for biofouling mitigation. *Desalination* **2015**, *356*, 187−207.
(48) Baerlocher, C.; McCusker, L. B.; Olson, D. H. *Atlas of zeolite framework types*; Elsevier: Amsterdam, 2007.
(49) Treacy, M.; Rivin, I.; Balkovsky, E.; Randall, K.; Foster, M. Enumeration of periodic tetrahedral frameworks. II. Polynodal graphs. *Microporous Mesoporous Mater.* **2004**, *74*, 121−132.
(50) Deem, M. W.; Pophale, R.; Cheeseman, P. A.; Earl, D. J. Computational discovery of new zeolite-like materials. *J. Phys. Chem. C* **2009**, *113*, 21353−21360.
(51) Pophale, R.; Cheeseman, P. a.; Deem, M. W. A database of new zeolite-like materials. *Phys. Chem. Chem. Phys.* **2011**, *13*, 12407.
(52) Li, L.; Dong, J.; Nenoff, T. M.; Lee, R. Desalination by reverse osmosis using MFI zeolite membranes. *J. Membr. Sci.* **2004**, *243*, 401−404.
(53) Kazemimoghadam, M.; Mohammadi, T. Synthesis of MFI zeolite membranes for water desalination. *Desalination* **2007**, *206*, 547−553.
(54) Li, L.; Liu, N.; McPherson, B.; Lee, R. Influence of counter ions on the reverse osmosis through MFI zeolite membranes: Implications for produced water desalination. *Desalination* **2008**, *228*, 217−225.
(55) Duke, M. C.; O'Brien-Abraham, J.; Milne, N.; Zhu, B.; Lin, J. Y.; Diniz da Costa, J. C. Seawater desalination performance of MFI type membranes made by secondary growth. *Sep. Purif. Technol.* **2009**, *68*, 343−350.
(56) Kazemimoghadam, M. New nanopore zeolite membranes for water treatment. *Desalination* **2010**, *251*, 176−180.
(57) Khajavi, S.; Jansen, J. C.; Kapteijn, F. Production of ultra pure water by desalination of seawater using a hydroxy sodalite membrane. *J. Membr. Sci.* **2010**, *356*, 52−57.
(58) Dong, H.; Qu, X. Y.; Zhang, L.; Cheng, L. H.; Chen, H. L.; Gao, C. J. Preparation and characterization of surface-modified zeolite-polyamide thin film nanocomposite membranes for desalination. *Desalin. Water Treat.* **2011**, *34*, 6−12.
(59) Lin, Y.; Duke, M. C. Recent progress in polycrystalline zeolite membrane research. *Curr. Opin. Chem. Eng.* **2013**, *2*, 209−216.
(60) Zhu, B.; Kim, J.; Na, Y.-H.; Moon, I.-S.; Connor, G.; Maeda, S.; Morris, G.; Gray, S.; Duke, M. Temperature and pressure effects of desalination using a MFI-type zeolite membrane. *Membranes* **2013**, *3*, 155−168.

DOI: 10.1021/acs.jpcc.7b00214
J. Phys. Chem. C XXXX, XXX, XXX−XXX

(61) Garofalo, A.; Donato, L.; Drioli, E.; Criscuoli, A.; Carnevale, M.; Alharbi, O.; Aljlil, S.; Algieri, C. Supported MFI zeolite membranes by cross flow filtration for water treatment. *Sep. Purif. Technol.* **2014**, *137*, 28−35.
(62) Zhu, B.; Hong, Z.; Milne, N.; Doherty, C. M.; Zou, L.; Lin, Y.; Hill, A. J.; Gu, X.; Duke, M. Desalination of seawater ion complexes by MFI-type zeolite membranes: Temperature and long term stability. *J. Membr. Sci.* **2014**, *453*, 126−135.
(63) Zhu, B.; Myat, D. T.; Shin, J.-W.; Na, Y.-H.; Moon, I.-S.; Connor, G.; Maeda, S.; Morris, G.; Gray, S.; Duke, M. Application of robust MFI-type zeolite membrane for desalination of saline wastewater. *J. Membr. Sci.* **2015**, *475*, 167−174.
(64) Huang, H.; Qu, X.; Dong, H.; Zhang, L.; Chen, H. Role of NaA zeolites in the interfacial polymerization process towards a polyamide nanocomposite reverse osmosis membrane. *RSC Adv.* **2013**, *3*, 8203−8207.
(65) Kim, S. G.; Hyeon, D. H.; Chun, J. H.; Chun, B.-H.; Kim, S. H. Nanocomposite poly(arylene ether sulfone) reverse osmosis membrane containing functional zeolite nanoparticles for seawater desalination. *J. Membr. Sci.* **2013**, *443*, 10−18.
(66) Pendergast, M. M.; Ghosh, A. K.; Hoek, E. Separation performance and interfacial properties of nanocomposite reverse osmosis membranes. *Desalination* **2013**, *308*, 180−185.
(67) Hosseini, S.; Rafiei, S.; Hamidi, A.; Moghadassi, A.; Madaeni, S. Preparation and electrochemical characterization of mixed matrix heterogeneous cation exchange membranes filled with zeolite nanoparticles: Ionic transport property in desalination. *Desalination* **2014**, *351*, 138−144.
(68) Dong, H.; Zhao, L.; Zhang, L.; Chen, H.; Gao, C.; Winston Ho, W. High-flux reverse osmosis membranes incorporated with NaY zeolite nanoparticles for brackish water desalination. *J. Membr. Sci.* **2015**, *476*, 373−383.
(69) Cay-Durgun, P.; McCloskey, C.; Konecny, J.; Khosravi, A.; Lind, M. L. Evaluation of thin film nanocomposite reverse osmosis membranes for long-term brackish water desalination performance. *Desalination* **2017**, *404*, 304−312.
(70) Hughes, Z. E.; Carrington, L. A.; Raiteri, P.; Gale, J. D. A computational investigation into the suitability of purely siliceous zeolites as reverse osmosis membranes. *J. Phys. Chem. C* **2011**, *115*, 4063−4075.
(71) Han, K. N.; Bernardi, S.; Wang, L.; Searles, D. J. Water diffusion in zeolite membranes: Molecular dynamics studies on effects of water loading and thermostat. *J. Membr. Sci.* **2015**, *495*, 322−333.
(72) Liu, Y.; Chen, X. High permeability and salt rejection reverse osmosis by a zeolite nano-membrane. *Phys. Chem. Chem. Phys.* **2013**, *15*, 6817.
(73) Lin, J.; Murad, S. A computer simulation study of the separation of aqueous solutions using thin zeolite membranes. *Mol. Phys.* **2001**, *99*, 1175−1181.
(74) Turgman-Cohen, S.; Araque, J. C.; Hoek, E. M. V.; Escobedo, F. A. Molecular dynamics of equilibrium and pressure-driven transport properties of water through LTA-type zeolites. *Langmuir* **2013**, *29*, 12389−12399.
(75) Plimpton, S. Fast parallel algorithms for short-range molecular dynamics. *J. Comput. Phys.* **1995**, *117*, 1−19.
(76) Humphrey, W.; Dalke, A.; Schulten, K. VMD: Visual molecular dynamics. *J. Mol. Graphics* **1996**, *14*, 33−38.
(77) Emami, F. S.; Puddu, V.; Berry, R. J.; Varshney, V.; Patwardhan, S. V.; Perry, C. C.; Heinz, H. Force field and a surface model database for silica to simulate interfacial properties in atomic resolution. *Chem. Mater.* **2014**, *26*, 2647−2658.
(78) Cruz-Chu, E. R.; Aksimentiev, A.; Schulten, K. Water-silica force field for simulating nanodevices. *J. Phys. Chem. B* **2006**, *110*, 21497−21508.
(79) Lopes, P. E. M.; Murashov, V.; Tazi, M.; Demchuk, E.; MacKerell, A. D. Development of an empirical force field for silica. Application to the quartz−water interface. *J. Phys. Chem. B* **2006**, *110*, 2782−2792.
(80) Joung, I. S.; Cheatham, T. E. Determination of alkali and halide monovalent ion parameters for use in explicitly solvated biomolecular simulations. *J. Phys. Chem. B* **2008**, *112*, 9020−9041.
(81) Allen, M. P.; Tildesley, D. J. *Computer simulation of liquids*; Oxford University Press: New York, 1989.
(82) Sartbaeva, A.; Wells, S. a.; Treacy, M. M. J.; Thorpe, M. F. The flexibility window in zeolites. *Nat. Mater.* **2006**, *5*, 962−965.
(83) Schatzberg, P. Molecular diameter of water from solubility and diffusion measurements. *J. Phys. Chem.* **1967**, *71*, 4569−4570.
(84) Willems, T. F.; Rycroft, C. H.; Kazi, M.; Meza, J. C.; Haranczyk, M. Algorithms and tools for high-throughput geometry-based analysis of crystalline porous materials. *Microporous Mesoporous Mater.* **2012**, *149*, 134−141.
(85) Marcus, Y. Ionic radii in aqueous solutions. *Chem. Rev.* **1988**, *88*, 1475−1498.
(86) Tzanis, L.; Marler, B.; Gies, H.; Patarin, J. High-pressure water intrusion investigation of pure silica ITQ-7 zeolite. *J. Phys. Chem. C* **2013**, *117*, 4098−4103.
(87) Humplik, T.; Raj, R.; Maroo, S. C.; Laoui, T.; Wang, E. N. Effect of hydrophilic defects on water transport in MFI zeolites. *Langmuir* **2014**, *30*, 6446−6453.
(88) Ohio Supercomputer Center. http://osc.edu/ark:/19495/f5s1ph73 (accessed 1987).

DOI: 10.1021/acs.jpcc.7b00214
J. Phys. Chem. C XXXX, XXX, XXX−XXX